Bulletin of the National
Research Centre

## RESEARCH

# Structural basis to identify a target site in Shiga toxin for the inhibitor discovery against growth of Shiga toxin-producing *E. coli*

Anuja Prabhudesai[1], Samir Shaikh[1], Kayasth Zarna Ashwinbhai[1] and Reeshu Gupta[1*]

## Abstract

**Background**  Certain peptides that bind Shiga toxin 2 (Stx2) have been reported to treat Shiga toxin-producing *Escherichia coli* (STEC) infections. However, their mechanisms of action remain unknown. STEC infections lead to serious diseases, such as hemolytic uremic syndrome, in humans. Antibiotic therapy is usually not recommended because of the major challenges of antibiotic resistance and SOS repair. Currently, there is no human vaccine for STEC infection, leaving rehydration therapy as the recommended supportive therapy. Therefore, there is a need for targeted therapeutic intervention to inhibit STEC growth. The purpose of this study was to evaluate the interaction of five known peptides with Stx2 to identify a more suitable peptide based on structural changes. These peptides have been used to inhibit the growth of STEC.

**Results**  The current study demonstrated that only tetravalent peptide (TVP) out of 5 common peptides interrupted the Y77-E259 interaction of Stx2, making it active by exposing active site, which ultimately leads to STEC cell death. We also demonstrated that amino acids R170 and F171 of Stx2 in the docked complex of Stx2 and TVP form a helix-loop-helix (HLH). This might lead to the differential expression of genes regulated by Stx2 and ultimately inhibit STEC growth. However, in the case of Stx2-ribosomal P-stalk, these residues did not form HLH. The 3D refined model of TVP showed a low MolProbity score and low energy zones in the ANOLEA profile compared to the original one. Moreover, the low radius of gyration of the refined TVP suggests that it is more compact than the original TVP. Therefore, TVP is a suitable drug candidate for the inhibition of STEC growth. However, the low antigenicity of TVP makes it unsuitable as a drug candidate. We also evaluated three antibiotics that have been used as active ingredients in FDA-approved peptides. Only Oritavancin diphosphate showed strong polar interactions with Y77-E259 and also had the highest binding affinity.

**Conclusions**  Potential drug candidates that inhibit or interrupt the interaction between Y77-E259 and have high antigenicity, low toxicity, and no allergenicity should be explored against the growth of STEC.

**Keywords**  Shiga toxin-producing *E. coli*, Tetravalent peptide, Antibiotics, Ribosome binding site, Ribosomal P-stalk

## Background

Shiga toxin-producing *Escherichia coli* (STEC) are a heterogeneous group of *E. coli* strains that produces Shiga toxins (Stxs). STEC infections are associated with various diseases such as diarrhea, hemorrhagic colitis (HC), hemolytic uremic syndrome (HUS) in humans, gastrointestinal sickness, edema disease in pigs, wildlife infections, calf mortality, diarrhea, and dysentery in calves (Chase-Topping et al. 2023; Deep et al. 2023; Fernandez

*Correspondence:
Reeshu Gupta
reeshu.gupta25198@paruluniversity.ac.in
[1] Centre of Research for Development Cell, Parul Institute of Applied Sciences, Parul University, Vadodara 391760, India

et al. 2023; Fitzgerald et al. 2023; Freedman et al. 2023; Jones et al. 2023; Liu et al. 2023; Neu et al. 2023; Tang et al. 2023). Currently, the recommended therapy for STEC infection is supportive, such as rehydration therapy (Muhlen and Dersch 2020). The treatment of STEC infection with antibiotics is controversial for two main reasons: (1) antibiotic resistance (Heydari et al. 2020; Milton et al. 2023; Oguadinma et al. 2023; Rubab and Oh 2021) and (2) induction of SOS repair (Crane et al. 2021). Therefore, antibiotics are not usually recommended for STEC infections (Kakoullis et al. 2019; Tarr and Freedman 2022). However, certain antibiotics, such as rifampicin in the presence of an STEC-specific phage cocktail, do not induce the release of phages from the genome of the STEC strain, which makes it a promising anti-STEC agent(s) (Necel et al. 2022). Other strategies for the treatment of STEC infections include antibody therapy, extracellular vesicles, vaccines, toxin receptor analogs, and plants or natural products (Caballero-Prado et al. 2021; Henrique et al. 2022; Lee et al. 2023).

New therapeutic approaches and strategies have recently been developed to manage STEC infections in recent years. For example, therapeutic peptides interfere with intracellular Stx trafficking and successfully prevent Stx2 toxicity (Rahal et al. 2015), (Biernbaum et al. 2023; Li et al. 2016; Lino et al. 2011; Prada-Prada et al. 2020; Stearns-Kurosawa et al. 2011; Watanabe-Takahashi et al. 2021). For example, Ac-PPP-tet and TVP contain four Pro-Pro-Pro-Arg-Arg-Arg-Arg motifs. PPP-tet was shown to protect mice from fatal doses of *E. coli* O157:H7 (Nishikawa et al. 2006). The addition of acetyl groups renders this compound resistant to proteolysis during STEC infection. These data indicate that Ac-PPP-tet is a promising therapeutic agent for STEC infections. However, characterization of these peptides and the mechanism of their interaction with Stx2 have not been thoroughly investigated.

There are two types of Stxs: Stx1 and Stx2. Stx2 is more toxic and has two subunits, A (holotoxin) and B. Glycolipid globotriaosylceramide (Gb3, CD77) acts as a receptor for B subunit. These receptors are present in various human cells such as glomerular and brain endothelial cells. After binding, the holotoxin is internalized by endocytosis, and the A1 and A2 fragments are formed due to proteolytically cleavage of the A subunit (Rudolph et al. 2020). The A1 subunit removes adenine from the highly conserved sarcin/ricin loop (SRL) in 28S rRNA, thereby inhibiting protein synthesis (de Virgilio et al. 2010). The active and ribosomal binding sites of Stx2 are located on opposite sides of the A1 subunit of Stx2 (Stx2A1) (Li and Tumer 2017). According to a previous report, the Stx2A1 subunit binds to the C-terminus of ribosomal P-stalk proteins via R172, R176, and R179

but does not remove adenine from SRL because their active sites (Tyr76/Tyr77, Tyr114, Glu167, and Arg170) are blocked (Li and Tumer 2017). This shows that removing the blockage of active sites is essential for depurination of SRL or inhibition of protein synthesis. However, information regarding the specific active sites has not been studied in detail. Interestingly, Stxs attack bacterial ribosomes as effectively as eukaryotic ribosomes, making them potential targets for the development of drugs against STEC (Suh et al. 1998). Hence, it is difficult to purify Stx2A from *E. coli* because it can attack the bacterial ribosomes (Rudolph et al. 2020).

The current bioinformatics approach used in this study demonstrated that blockage of Y77-E259 and Y114-E167 interactions is required to activate Stx2 by exposing its active site. These interactions were evaluated in five known peptides that have been used against STEC growth. While all peptides interacted with Y77 and E259, only one TVP (MAPPPRRRRA) interrupted the interaction between Y77 and E259 residues of Stx2A1, rendering Stx2 active by exposing the active site, ultimately leading to STEC cell death. We also showed a change in the structural conformation of the Stx2A-TVP complex compared to the Stx-2-ribosome p-stalk protein complex. However, its low antigenicity and negative G-factor make it an unsuitable drug candidate. Therefore, potential candidates that inhibit the interaction of Y77-E259 should be explored against the growth of STEC.

## Methods
### Bioinformatics analysis
The structures of Stx2 (PDB ID:7D6Q) and Stx2-ribosomal P-stalk proteins (PDB ID:7U6V) were downloaded in the PDB format. The PEP-FOLD server at the RPBS MOBYLE portal was used to determine the 3-D structure of therapeutic peptides against STEC infections (Thevenet et al. 2012). In this server, the amino acid sequence is provided in the FASTA format. These amino acids must include 20 standard amino acids. The server can not be used for the peptides longer than 50 amino acids and thus, has limitations. Docking between Stx2 and therapeutic peptides was performed using the Clus-Pro server (Comeau et al. 2004). The server has inherent problems of new additions and size of proteins submitted. The receptor protein can be no larger than 11,999 atoms and the ligand can be no larger than 4700 atoms after minimization (Comeau et al. 2004). Proteins and ligands were prepared using UCSF chimera as described previously (Pettersen et al. 2004; Sameer et al. 2023). The iMODS online server was used on the Stx2-TVP docking complex to perform a Normal Mode Analysis (NMA) (Lopez-Blanco et al. 2014). iMODS was used to generate the covariance matrix of the docking complex. The

ERRAT method (Colovos and Yeates 1993) was used to detect incorrect regions, and the PROCHECK server through a Ramachandran plot (Laskowski et al. 1996) was used to predict the stereochemical quality validation of the Stx2-TVP complex. The structures of three antibiotics (active ingredients of FDA-approved peptides) (Chen and Lu 2020), Oritavancin diphosphate (CID:53297457), telavancin hydrochloride (CID:53297457), and daptomycin (CID:16134395), were downloaded from PubChem for docking studies. Molecular docking between stx2 and these antibiotics was performed using PyRx (Dallakyan and Olson 2015). The visualization tool, PyMOL, was used to observe the interactions of Stx2 with TVP and active ingredients of FDA-approved peptides.

### Physiochemical property analysis of the TVP
Physiochemical properties of therapeutic peptides were computed using 'peptides' package of RStudio and Prot-Param (Gasteiger et al. 2003). It predicts ten structural characteristics of antimicrobial peptides (AMP), including length, amino acid composition, molecular weight, net charge, isoelectric point, extinction coefficient, aliphatic index, instability index, potential peptide interaction index (Boman index), hydrophobic moment, and GRAVY hydrophobicity index (Gupta et al. 2013; Wilkins et al. 1999). The characteristic properties of effective AMP are their short length ($<10$ kDa, 10–15 amino acid residues long), net positive charge of at least $+2$ at pH 7, and amphipathic nature. A positive net charge on AMP predicts its binding specificity to negatively charged bacterial membranes. The extinction coefficient measures how strongly a protein absorbs or reflects light of a specific wavelength. The aliphatic index of a protein is related to the thermal stability of the protein. An instability index value of $>40$ indicates instability. The Boman index differentiates the mechanism of action of antimicrobial peptides (protein membranes). A high value of the Boman index denotes its interaction with other proteins, while a negative value denotes no interaction with other proteins during their mechanism of action. Positive values of the hydrophobicity index and GRAVY indicate that the peptide can cross the cell membrane.

### Evaluation of the 3D refined model
The structure of TVP (MAPPPRRRRA) was refined using the GalaxyRefine server (Ko et al. 2012) and evaluated for its stereochemical properties using a Ramachandran plot (Laskowski et al. 1996). Tools such as the QMEAN6 server (Qualitative Model Energy Analysis) were used to predict the quality of the models at the global and local levels (Benkert et al. 2009). The ANOLEA profile was created for the refined and original TVP to calculate the areas of high energy (Melo et al. 1997). The simulation was performed using the CHARMM force field between the refined and original models of the TVP with stx2, using GROMACS version 2022.5. System build-in commands were used for solvation, ion addition, and energy minimization. The simulation was performed for 100 ns, and the root-mean-square deviation (RMSD) and radius of gyration (Rg) were calculated for both the original and refined TVP. The statistical differences in RMSD and Rg were assessed by applying one-way analysis of variance followed by Bonferroni post-hoc test using OriginPro (Version:2019b) software. $P < 0.05$ was considered statistically significant.

### Antigenicity, allergenicity and toxicity analysis
Antigenicity prediction was done using the VaxiJen v2.0, server (Doytchinova and Flower 2007). Using this approach, only those proteins were selected for further evaluation which had antigenicity scores higher than the threshold value of 0.4. AllergenOnline was used to identify allergic actions (Goodman et al. 2016). The server predicted allergenicity using six different approaches. However, the best approach is a BLAST search for allergen representative peptides because of its high accuracy, sensitivity, and specificity. ToxinPred was used to study the toxicity of the TVP (Gupta et al. 2013).

## Results
### Evaluation of the Stx2 and Stx2-ribosomal P-stalk
It has been shown that the position of glutamate 259 (E259) likely blocks the interaction of Stx2 with SRL, rendering it catalytically inactive (Rudolph et al. 2020). We first studied the interaction between Y77 and E259 in the cryo-EM structure of Stx2A1 in complex with the native ribosomal P-stalk (PDB ID:7U6V). In this structure, Y77-E259 and Y114-E167 were located far from each other and did not exhibit polar interactions (Fig. 1A, B). However, in Stx2 (PDB:7D6Q), these residues interacted via hydrogen bonding (Fig. 1C, D). These results suggest that the interaction of Stx2 with the ribosome p-stalk blocks or inhibits Y77-E259 and Y114-E167 interactions.

### Effect of Shiga toxin associated peptides on the Y77-E259 and Y114-E167 interactions
Docking analysis of the Stx2-peptides complexes revealed that out of the five known peptides, only one TVP (MAPPPRRRRA) blocked the interaction between the Y77 and E259 residues of Stx2A1 (Fig. 2 and Table 1). Therefore, it makes Stx2 catalytically active by exposing its active site (Y77), resulting in the inhibition of bacterial ribosomes. However, all peptides showed a close interaction with the Y77 and E259 residues of stx2A1 (data not shown), suggesting the role of interaction of peptides with these residues in STEC killing.
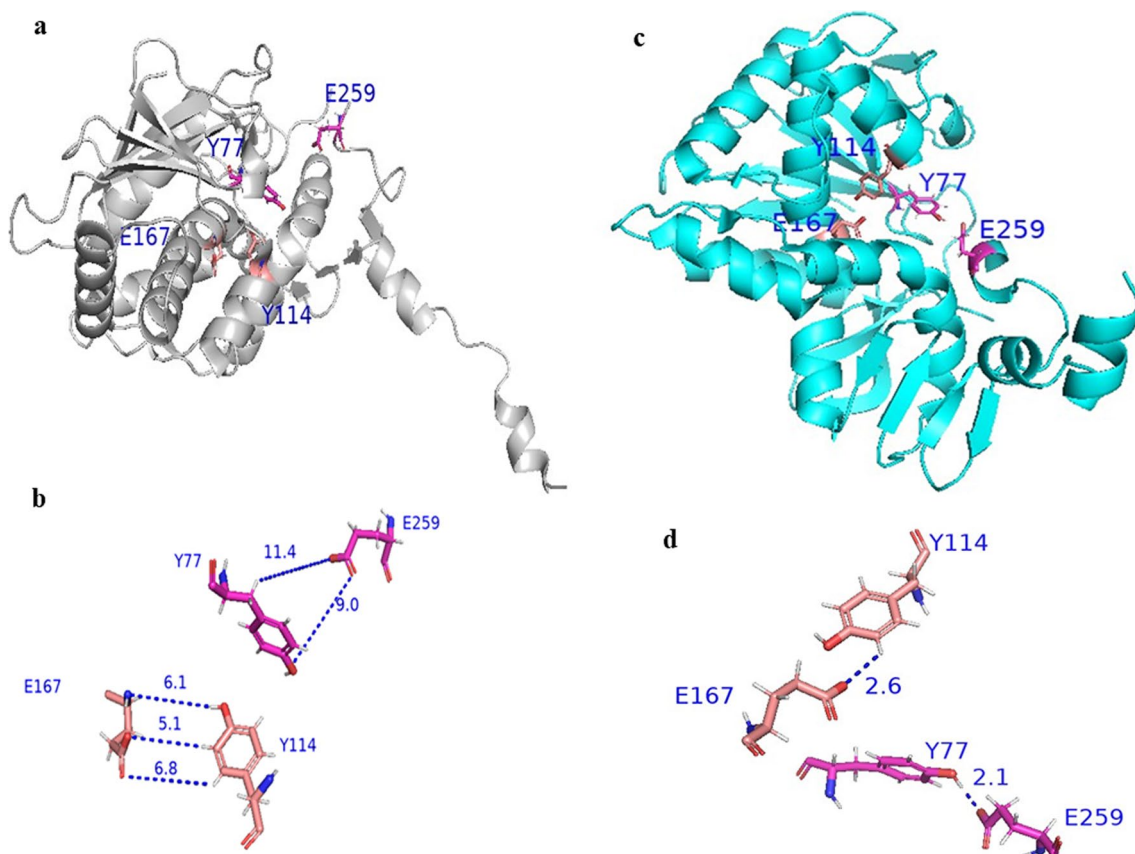
**Fig. 1** Docking analysis showing interactions of tyrosine 77 (Y77)-glutamate 259 (E259) (magenta, stick) and tyrosine 114-glutamate 167 (E167) (purple, stick) in the complex of Stx2-ribosomal P-stalk (gray), **a** cartoon model depicting interactions of Y77 and E259 in the complex of Stx2-ribosomal P-stalk, **b** hydrogen bonding between Y77 and E259 in Stx2-ribosome P-stalk. **c, d** Docking analysis showing interactions of tyrosine 77 (Y77)-glutamate 259 (E259) (magenta, stick) and tyrosine 114-glutamate 167 (E167) (purple, stick) in the complex of Stx2 (cyan), **c** cartoon model depicting interactions of Y77 and E259 in the complex of Stx2, **d** hydrogen bonding between Y77 and E259 in Stx2. Blue colored dashes are showing hydrogen bonding. Amino acids were labeled using a one-letter code
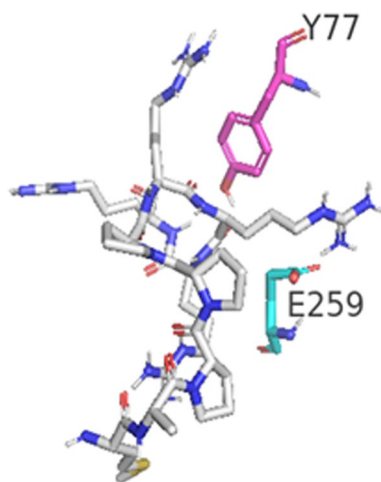


**Fig. 2** Interaction of the TVP (gray, stick) with Y77 (magenta, stick) and E259 (cyan, stick) of Stx2

The binding pocket of TVP was predicted by the CASTp 3.0 available online at http://cast.engr.uic.edu (Tian et al. 2018). The binding pocket is lined by chains A, D, and E of Stx2 (Fig. 3A,B). The area and volume of the binding pocket was $381.6A^{\circ 2}$ and $191.5A^{\circ 3}$, respectively. Amino acids occupying the binding pocket are shown in Fig. 3C. TVP exhibited hydrogen bonding with E72, Y77, V78, S112, T115, Q257, and E259 in chain A and K7 and D70 in chain D, whereas hydrophobic interactions were formed by N74, N75, Y114, Q118, R125, V162, E167, R170, T199, L200, W202, L239, Q261, and I262 in chain A, and K7, I8, E9, K22, Q43, and G46 in chain D of Stx2 (Fig. 4A, B).

The covariance matrix indicates that Y77 and E259 show anti-correlated motion (blue region), which indicates that Y77 and E259 are moving far from each other after interaction with the TVP (Fig. 5A). The Ramachandran plot showed that 92.9% and 7.1% of residues were in the favored and allowed regions, respectively. No

**Table 1** Evaluation of the polar interaction of therapeutic peptides with Stx2

| SN | Name | HPEPDOCK score | ClusPro score | Amino acids residues of Stx2 showing polar interaction with peptide | Whether blocking Y77-E259 or Y114-E167 interaction |
|----|------|----------------|---------------|----------------------------------------------------------------------|---------------------------------------------------|
| 1 | WRWYCRR (Lino et al. 2011) | − 229.232 | − 964.8 | **Y77,** D94, **Y114, E167,** R170, F171, L200, P258, **E259**, Q261, I262 | No |
| 2 | TFNMWLPTFNQW (Li et al. 2016) | − 206.687 | − 877.7 | **Y77**, D94, W202, G203, R204, **E259**, N279 | No |
| 3 | MMARRRR (Watanabe-Takahashi et al. 2021) | − 183.481 | − 748.5 | **Y77**, D94, D111, S112, **Y114**, R170, L200, **E259** | No |
| 4 | MAPPPRRRRA (Stearns-Kurosawa et al. 2011) | − 182.587 | − 576.5 | E72, **Y77**, V78, S112, G203, Q257, **E259**; Chain D-K7, D70 | Yes (only block Y77-E259) |
| 5 | EWGRRMMGRGPGRRMMRWWR (Prada-Prada et al. 2020) | − 213.327 | − 900.1 | E72, **Y77**, **Y114**, T199, L200, G203, **E259**, Q261 | No |

Bold indicated y77, E259, and Y114, E167 are interacting with each other in Stx2, however, peptides are interacting with these peptides and inhibiting the interaction
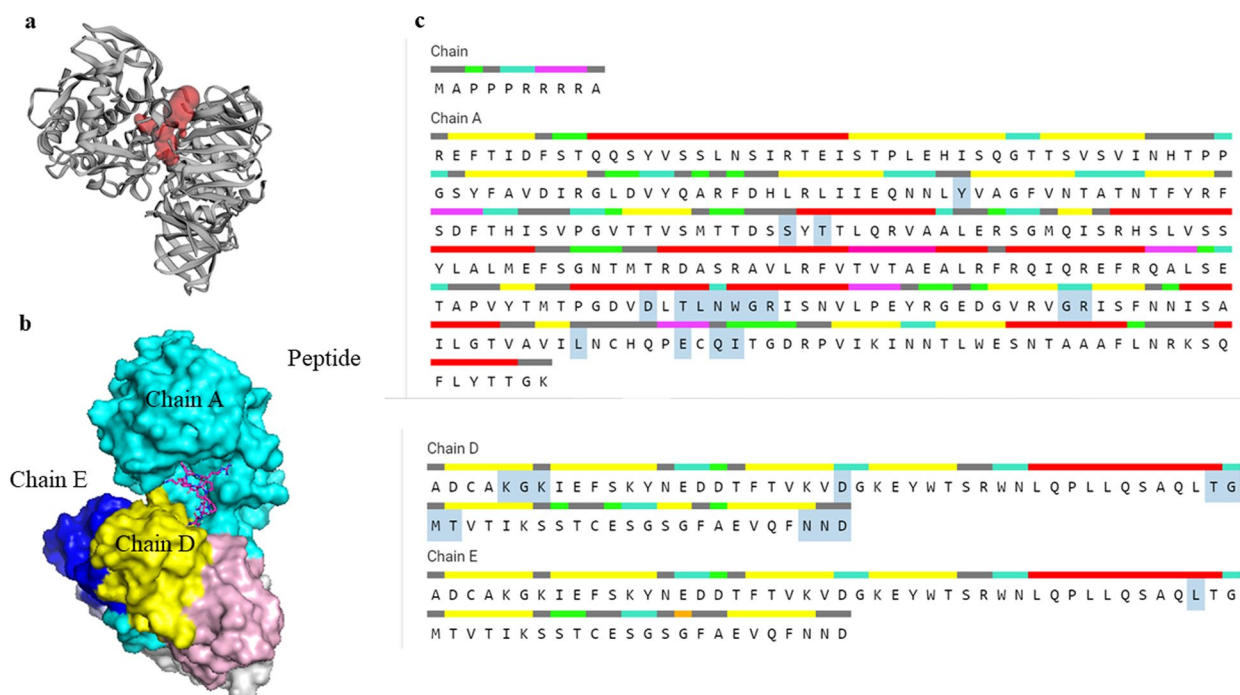


**Fig. 3** Structural model depicting the presence of TVP in the binding pocket of Stx2. **a** Binding site of peptide indicated by red region, **b** Binding pocket surrounded by chains A (cyan), D (yellow), and E (blue) of Stx2. **c** Amino acids occupying the binding pocket are shown in gray colored shaded region

residues were found in outlier regions (Fig. 5B). However, the overall G-factor value was slightly negative (− 0.05), indicating residues in slightly unlikely conformations. The structure was also validated using another structure verification server called Errat, which showed an overall quality factor of 83.36 for Stx2-TVP. In ERRAT, an error value exceeding the 99% confidence level indicates a poorly modeled region. For both Y77 and E259, the error values were below the 50% confidence level, indicating

that these residues are present in the optimal model region of the Stx2-TVP complex (Fig. 6).

**Effect of TVP on the ribosome binding sites of Stx2**

PyMOL was used to superimpose the structures of Stx2-TVP and Stx2-ribosomal P-stalk (Fig. 7A). The region near the ribosomal binding site (R172, R176, and R179) of Stx2 was also studied (Fig. 7B). Structural analysis of the Stx2-TVP complex demonstrated that two residues
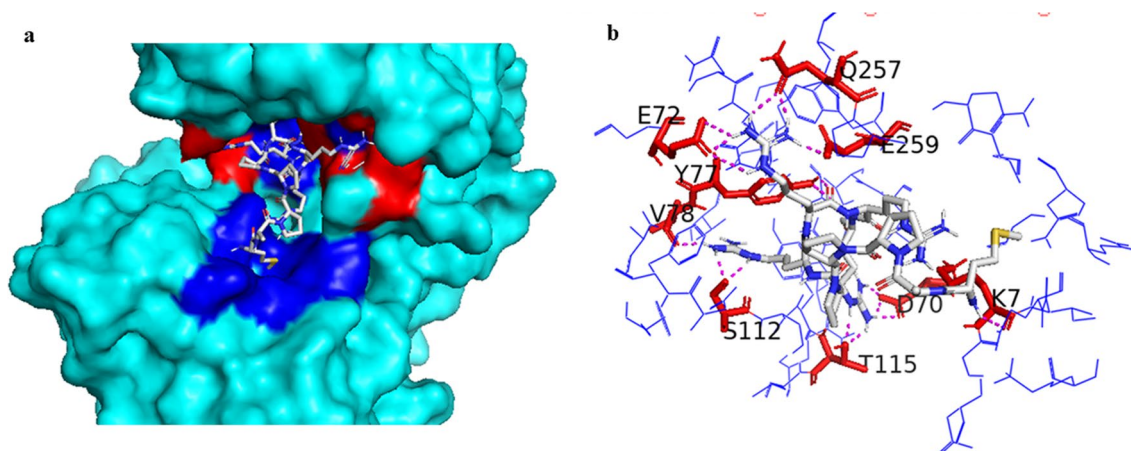
**Fig. 4** Molecular docking of Stx2-TVP complex, **a** Surface model depicting the hydrogen bonding (red) and hydrophobic interactions (blue) between TVP (gray) and Stx2 (cyan) in the binding pocket, **b** Hydrogen bonding between active residues (red; sticks) of Stx2 with TVP (gray, sticks) and hydrophobic interactions between amino acid residues (blue, lines) of Stx2 with peptide. Magenta colored dashes are showing hydrogen bonding. Amino acids were labeled using a one-letter code
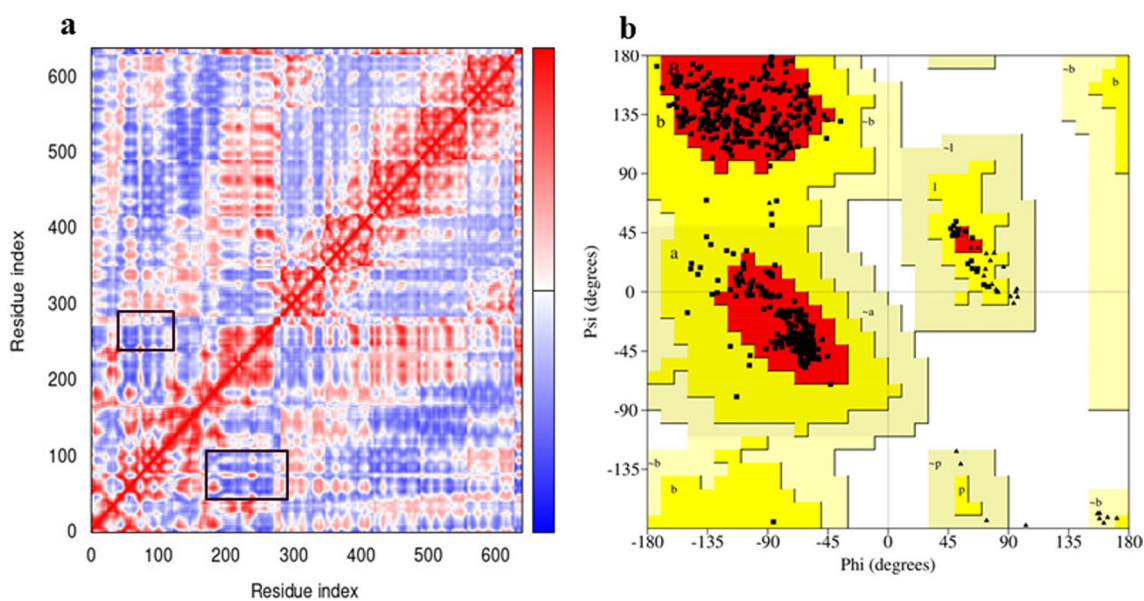


**Fig. 5 a** Covariance matrix indicate coupling between residues, where red represents correlated, white represents uncorrelated and blue represents anti-correlated motions of residues. Black boxes represent relative movement of residues positioned at 50–100 or 250–300. These regions covered the Y77 and E259 regions. **b** Ramachandran plot of the Stx2-TVP complex. The red-colored boxes represent most favored regions. Additional allowed regions are denoted by yellow color boxes

(R170 and F171) located near ribosomal binding sites (RBS) were present in the loop of the A subunit of Stx2 (Fig. 7C). Loops containing R170 and F171 are present between the two alpha helices (helix-loop-helix, HLH). HLH functions as a transcription factor that binds DNA and regulates gene expression (Massari and Murre 2000; Obata et al. 2022). However, in the case of Stx2-ribosomal P-stalk, these residues were located in the α-helix region of Stx2A1 (Fig. 7D).

**Secondary structure analysis**

The secondary structure of TVP was predicted using SOPMA server (Geourjon and Deleage 1995). It predicts the secondary structure based on the availability of amino acid sequences in the databases. The results showed that TVP was composed of 100% random coils (Fig. 8A). The Ramachandran plot showed that 60% and 40% of residues were in the favored and allowed regions, respectively. However, none of the residues was present in the outlier
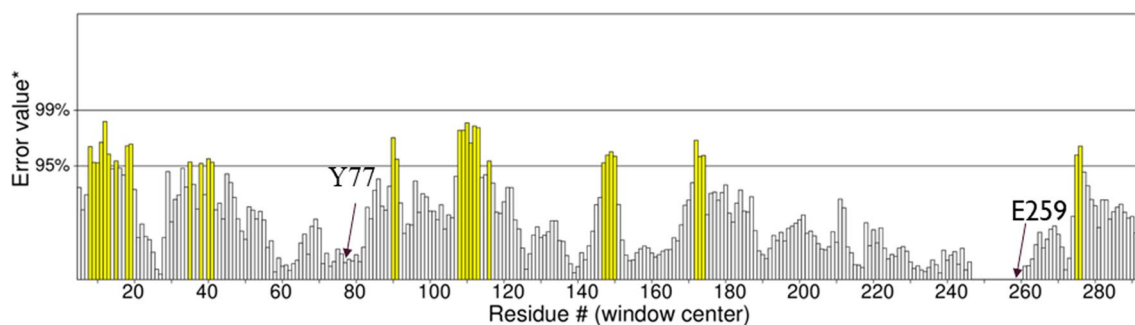
**Fig. 6** ERRAT plot showing the error values for residues in the Stx2-TVP complex. An error value exceeding the 99% confidence level indicates a poorly modeled region. The arrow indicates the error value at the < 50% confidence level for Y77 and E259
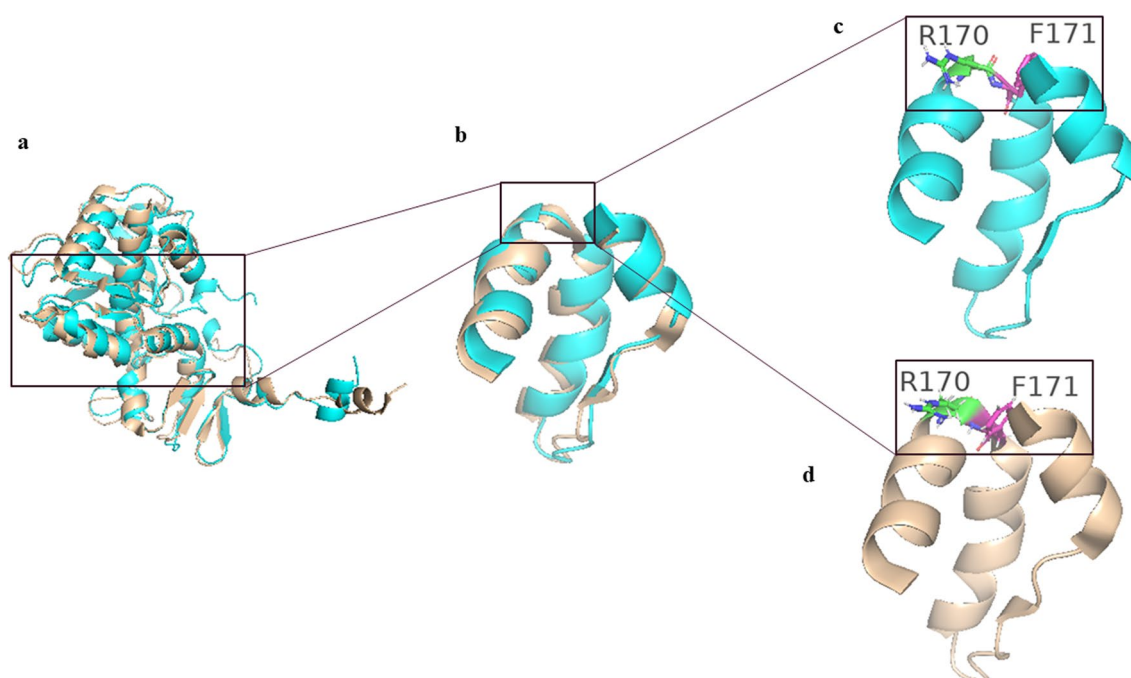


**Fig. 7** **a** Superimposition of Stx2-TVP (cyan) and Stx2-ribosomal P-stalk (golden), **b** Closer view of the superimposed structure near the ribosome binding sites (R172, R176, and R179) of **c** Stx2-TVP and **d** Stx2-ribosomal P-stalk depicting the presence of R170 (green, stick) and F171 (magenta, stick) in loop and helix, respectively. Amino acids were labeled using a one-letter code

region. According to the PROCHECK analysis, the overall G-factor of TVP was −0.55. The G-factor predicts the distance of each residue from the normal region of a plot. Negative G-factors indicate that the residues are not in the likely conformations.

## Refinement of tertiary structure of TVP

The tertiary (3D) structure of the TVP was refined using the GalaxyRefine server. The accuracy of the model is defined by the GDA-HA, MolProbity, and clash scores. MolProbity score highlights steric clashes. Five models were generated using GalaxyRefine, of which Model

1 was selected because of its conformational properties. Additionally, for the refined model, GDT-HA was 0.8750, whereas MolProbity, clash score, and poor rotamers were 1.692, 15.5, and 0.0, respectively. The GDT-HA, MolProbity, clash score, and poor rotamers for the original model were 1, 1.742, 6.6, and 0, respectively. When compared with the other models, Model 1 was predicted to be the best refined model based on different scores. Moreover, the Ramachandran plot showed that 100% of the residues were in the favored region of the three-dimensional structure (Fig. 8B). The G-factor for this model was +0.28, indicating residues in likely
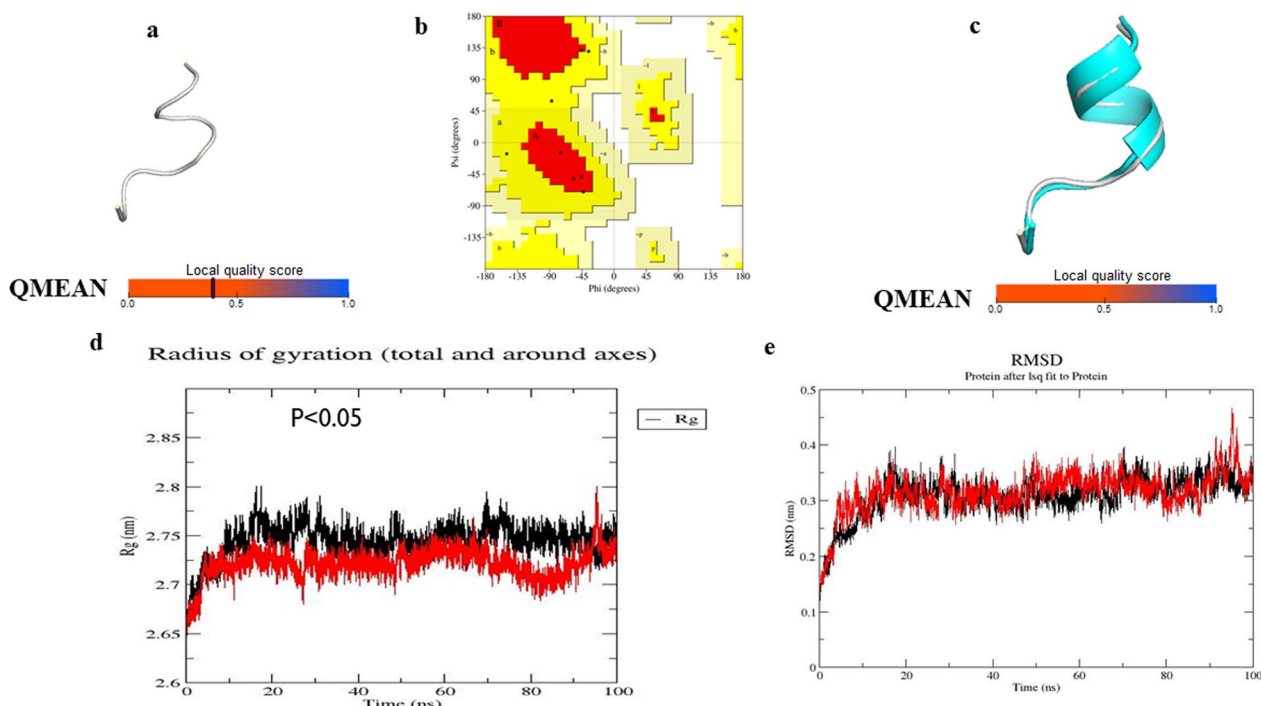
Prabhudesai *et al. Bulletin of the National Research Centre*       (2024) 48:35

Page 8 of 13



**Fig. 8** **a** Structure of the original TVP model. **b** Ramachandran plot of refined TVP. The most favored regions are denoted by red color. Additional allowed regions are denoted by yellow color, **c** Superimposition of original (gray) and refined (cyan) model of TVP, **d** Rg, **e** RMSD of original TVP (black) and refined TVP (red). *P* < 0.05 significant difference

conformations. Superimposition of the refined model with the original TVP showed differences in structural configuration (Fig. 8C). No significant changes were observed for the RMSD; however, the Rg was less for the refined model of TVP, suggesting more compactness of the refined structure (Fig. 8D, E).

Additionally, the QMEAN values (blue region) of the refined model are higher (0.67) than those of the original model (0.40), which indicates that the model scores are higher than those of the original model on average. In the ANOLEA profile, the initial model had many areas of high energy, which were greatly improved in the refined model, suggesting greater reliability (Fig. 9A, B).
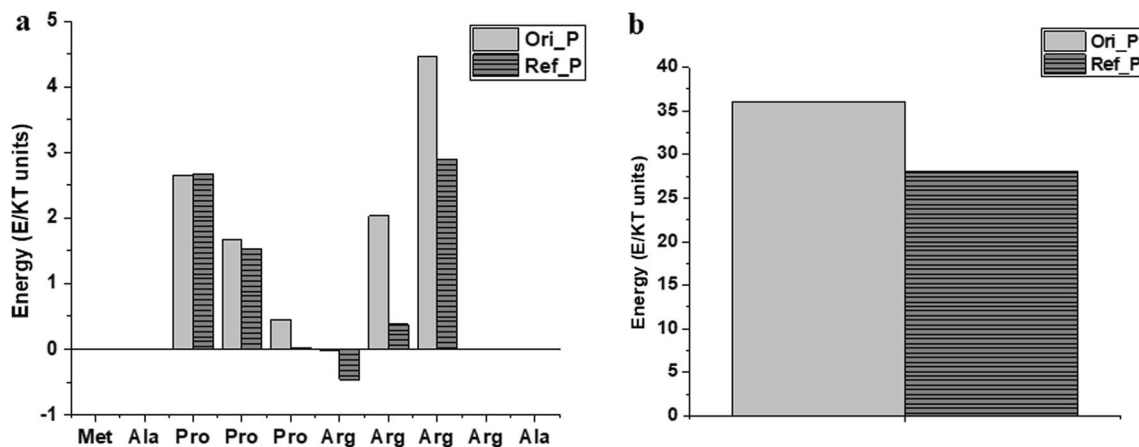


**Fig. 9** **a** ANOLEA plots showing energy zones of individual amino acids in original and refined TVP, **b** ANOLEA plot showing overall energy zone for original and refined TVP

## Physiochemical properties of tetravalent peptide

TVP has 174 atoms and its molecular weight was found to be 1.21 kDa. Further analysis showed that TVP had an isoelectric point (pI) value of 12.48, indicating its basic nature. The positive charge of TVP (+4) denotes its binding affinity for the negatively charged bacterial membranes. The amino acid composition showed the amphipathic nature of TVP, with four polar and six non-polar residues. Moreover, the membrane position of the TVP is globular, indicating its natural folding nature. These results suggest that TVP possesses characteristic properties that are essential for its effectiveness as an effective antimicrobial peptide. However, low aliphatic index and high instability index suggest that TVP is thermally unstable. Moreover, the hydrophobicity index and grand average of hydropathicity (GRAVY) were negative, indicating its hydrophilic nature (Table 2).

## Allergenicity, toxicity, and antigenicity analysis

Effective antimicrobial peptides do not have any allergenicity. No hits were found against the database of 2890 allergen representative peptides (ARPs), suggesting that all the five peptides were non-allergenic in nature.

ToxinPred analysis indicated the non-toxic nature of therapeutic peptides. Of the five peptides, only three had antigenic scores > 0.4, suggesting their protective antigenicity (Table 3) (Doytchinova and Flower 2007).

## Effect of antibiotics on the Y77-E259 and Y114-E167 interactions

Of the three antibiotics (active ingredients of FDA-approved peptides), only oritavancin diphosphate interacted with Y77, E259, and Y114 (Table 4). The same glycopeptide antibiotic exhibited the highest binding affinity. These analyses suggest a possible role of this antibiotic in the inhibition of STEC growth.

## Discussion

Antimicrobial peptides (AMPs) are small amino acid-based molecules that can kill various microorganisms at micromolar concentrations. AMPs were first identified in circulating phagocytes of humans (Spitznagel 1997). Later, they were identified in granulocytes, platelets, specialized epithelial glands, wet mucosal epithelial cells of the intestine, and fetal membranes. A variety of AMPs comprising an important part of the innate immune

**Table 2** Physiochemical attributes of TVP

| Property | Value |
|---|---|
| Number of amino acids | 10 (Tiny = 2, Small = 5, Aliphatic = 2, Polar = 2, non-polar = 6, charged = 4, Basic = 4) |
| Atomic composition | Carbon: 50 Hydrogen:90 Nitrogen:22 Oxygen:11 Sulfur:01 |
| Total number of negatively charged residues (Asp + Glu) | 0 |
| Total number of positively charged residues (Arg + Lys) | 4 |
| Formula | $C_{50}H_{90}N_{22}O_{11}S_1$ |
| Extinction coefficients | 0 (will not be visible by UV spectrophotometry) |
| Estimated half-life | > 30 h (mammalian reticulocytes, in vitro and > 10 h (Escherichia coli, in vivo) |
| Instability index | 243.42 |
| Aliphatic index | 20 |
| Grand average of hydropathicity (GRAVY) value | − 1.730 |

**Table 3** Antigenicity, allergenicity, toxicity and physiological attributes of therapeutic peptides

| SN | Name | Antigenicity score | Allergenicity | Toxicity | Boman index | GRAVY score |
|---|---|---|---|---|---|---|
| 1 | WRWYCRR (Lino et al. 2011) | 1.62 | No | No | 5.7 | − 2 |
| 2 | TFNMWLPTFNQW (Li et al. 2016) | 1.39 | No | No | 0.5 | − 0.3 |
| 3 | MMARRRR (Watanabe-Takahashi et al. 2021) | − 0.77 | No | No | 7.6 | − 1.8 |
| 4 | MAPPPRRRRA (Stearns-Kurosawa et al. 2011) | − 0.0045 | No | No | 5.4 | − 1.7 |
| 5 | EWGRRMMGRGPGRRMMRWWR (Prada-Prada et al. 2020) | 0.47 | No | No | 4.6 | − 1.7 |

**Table 4** Evaluation of the polar interaction of antibiotics with Stx2

| SN | Name | CID number | Binding affinity | Amino acids residues of Stx2 showing polar interaction with antibiotics | Whether blocking Y77-E259 or Y114-E167 interaction |
|---|---|---|---|---|---|
| 1 | Oritavancin diphosphate (Chen and Lu 2020) | 53297457 | − 14 | **Y77, Y114**, R125, L200, **E259** | No |
| 2 | TELAVANCIN HYDROCHLORIDE (Chen and Lu 2020) | 9812715 | − 14 | **Y114**, I271 | No |
| 3 | Daptomycin (Chen and Lu 2020) | 16134395 | − 11 | D94, S112, R204, Q261, I262, | No |

Bold indicated y77, E259, and Y114, E167 are interacting with each other in Stx2, however, peptides are interacting with these peptides and inhibiting the interaction

system have been identified, and an updated list is available in the data repository of antimicrobial peptides (DRAMP) (Bin Hafeez et al. 2021). AMPs have been shown to inhibit microbial growth prior to the recruitment of immune cells (Gallo and Nizet 2003).

Previous studies have shown that peptides are used to treat STEC infection (Rahal et al. 2015; Stearns-Kurosawa et al. 2011). Additionally, it was also shown that Stx2 can bind to the ribosome p-stalk but did not show activity due to blockage of the active site (Li and Tumer 2017). However, information about the active site and mechanism of action by which TVPs reduce STEC infection is unknown. This study demonstrated that TVP completely blocks the Y77-E259 interaction and thus exposes the Y77 active site, making Stx2 active. We also showed that structural conformation near the RBS of Stx2 changes in the presence of TVP and may affect gene expression regulated by Stx2 (Massari and Murre 2000; Obata et al. 2022). However, the negative G-factor and its non-antigenic nature likely make it an unsuitable drug candidate.

Antimicrobial agents such as antibiotics are also used to treat STEC infections. However, the use of these agents remains controversial. In some studies, antibiotics have been shown to enhance the risk of HUS; however, opposite results have also been reported. This may be related to the strains and antimicrobial agents used in their studies. There are various ways by which antibiotics can increase the release of Shiga toxin; for example, by developing resistance or by triggering a bacterial SOS response or other types of physiological stresses that activate the lytic cycle of the bacteriophage encoding Stx, thereby increasing Shiga toxin production (Hwang et al. 2021). Antibiotic resistance in STEC is due to the presence of plasmids carrying drug resistance genes. The unselective and uncontrolled use of antibiotics has encouraged the development of drug-resistant strains of STEC in animal and human populations. These antibiotic-resistant strains in animal populations can pose a global public health hazard due to their transmission from animals to humans. Ruminants, especially cattle, have been identified as major reservoirs of STEC (Boriollo et al. 2021). Antibiotics, such as azithromycin,

fosfomycin, and meropenem, are usually recommended for the treatment of early stage STEC infections. These antibiotics are known to prevent Shiga toxin release and kidney failure. However, antibiotic resistance can either reduce or negatively affect these treatment options (Mir and Kudva 2019). These studies suggest that treatment of STEC infections with antimicrobial agents should be reconsidered. For example, rifampicin and gentamycin together reduce Shiga toxin production (Puno-Sarmiento et al. 2020; Ramstad et al. 2021). It was also shown that a treatment of antibiotic-peptide combination reduces STEC infection without any effect on the release of Shiga toxins. This study suggests a strategy for the repurposing of antibiotics for treatment of STEC infection (Puno-Sarmiento et al. 2020).

In this study, only Oritavancin diphosphate formed polar interactions with Y77 and E259. However, it did not block the Y77-E259 interaction as in the case of TVP. This antibiotic has been classified by WHO as critically important to humans. Whether this binding creates an obstruction in the smooth interaction of Y77 with E259 needs to be validated by experimental work. Oritavancin is approved by the FDA for the treatment of acute bacterial skin and skin structure infections (SSSIs) in adults. SSSIs are suspected to be caused by gram-positive microorganisms, such as *Staphylococcus aureus* (methicillin-susceptible [MSSA] (Kumar et al. 2023) and methicillin-resistant [MRSA]), *Streptococcus pyogenes, Streptococcus agalactiae, Streptococcus dysgalactiae, Streptococcus anginosus* group (including *S. anginosus, Streptococcus intermedius*, and *Streptococcus constellatus*), and *Enterococcus faecalis* (vancomycin-susceptible isolates only) (Cada and Baker 2014). However, its role in STEC has not been evaluated. Overall, the current study suggests that potential drug candidates that can block the interaction between Y77-E259 should be explored against STEC growth.

## Conclusions

STEC poses health risks to animal reservoirs and food products with respect to easy transmission, causing outbreaks, and transferring resistance genes to

other pathogens in animals, humans, and plants (Al Qabili et al. 2022; Carter et al. 2023; El-Bastawisy et al. 2023). Therefore, prevention of STEC infection must be strengthened to avoid the spread of STEC. Despite the tremendous risks posed by *E. coli,* the emergence of antibiotic resistance has raised challenges in the treatment of STEC infections. Antibiotic treatment of STEC infections in humans is not usually recommended because they may worsen the disease by inducing toxin-related tissue damage and symptoms (Rubab and Oh 2021). Other strategies include antibody therapy, vaccines, toxin receptor analogs, and plants or natural products. Polyclonal antibodies have shown promising neutralizations in vitro and in vivo. However, animal sources of polyclonal antibodies may induce anti-antibody actions that inactivate therapeutic antibodies before showing toxin-neutralizing activity. Similarly, natural drugs have been tested in animal models, but not in clinical trials (Liu et al. 2022). Currently, there is no vaccine available for the treatment of STEC infections in humans (Liu et al. 2022). Therefore, it is imperative to identify new therapeutic approaches and strategies for managing STEC infection. In this study, only TVP interrupted the interactions between Y77 and E259 of the Stx2. This interruption exposes the active site (Y77) of Stx2, ultimately inhibiting STEC growth. Early studies have identified that Y77of Stx2 plays an important role in the catalytic activity of Stx2 (Di et al. 2011). The change in the structural conformation of the Stx2A-TVP complex forms HLH, which regulates differential gene expression and ultimately inhibits STEC growth. Therefore, the results of this study highlight the importance of interrupting the Y77-E259 interaction to inhibit STEC growth by TVP. However, TVP is an unsuitable drug candidate owing to its low antigenicity and negative G-factor. Additionally, the formation of insoluble toxic byproducts during peptide synthesis leads to adverse effects on the nervous, musculoskeletal, and cardiovascular systems. They can even cause cancer. Thus, the FDA has banned many peptides. Peptides also exhibit low bioavailability and metabolic liabilities. However, they cannot easily cross the epithelial barrier. Therefore, potential drug candidates that inhibit or interrupt the interaction between Y77-E259 should be explored against the growth of STEC. In this regard, three antibiotics were explored to evaluate their effects on the Y77-E259 interaction. Of the three antibiotics, only oritavancin diphosphate interacted with Y77, E259, and Y114, and exhibited the highest binding affinity. These analyses suggest a possible role of this antibiotic in the inhibition of STEC growth. It would be valuable to explore specific drug candidates or experimental approaches that can block or inhibit the Y77-E259 interaction.

## Abbreviations
TVP     Tetravalent peptide
STEC    Shiga toxin-producing *E. coli*
Stx2    Shiga toxin 2
SRL     Sarcin/ricin loop

## Availability of data and materials
The datasets used and/or analyzed during the current study are available from the corresponding author on reasonable request.

## Declarations

### Ethics approval and consent to participate
Not applicable.

### Consent for publication
Not applicable.

### Competing interests
The authors declare that they have no competing interests.

## References
Al Qabili DMA, Aboueisha AM, Ibrahim GA, Youssef AI, El-Mahallawy HS (2022) Virulence and antimicrobial-resistance of Shiga toxin-producing *E. coli* (STEC) Isolated from edible shellfish and its public health significance. Arch Microbiol 204(8):510. https://doi.org/10.1007/s00203-022-03114-2

Benkert P, Kunzli M, Schwede T (2009) QMEAN server for protein model quality estimation. Nucleic Acids Res 37(Web Server issue):W510–W514. https://doi.org/10.1093/nar/gkp322

Biernbaum EN, Dassanayake RP, Nicholson EM, Kudva IT (2023) Comparative evaluation of antimicrobial activity of human granulysin, bovine and porcine NK-lysins against Shiga toxin-producing *Escherichia coli* O157:H7. PLoS ONE 18(9):e0292234. https://doi.org/10.1371/journal.pone.0292234

Bin Hafeez A, Jiang X, Bergen PJ, Zhu Y (2021) Antimicrobial peptides: an update on classifications and databases. Int J Mol Sci. https://doi.org/10.3390/ijms222111691

Boriollo MFG, Moreira BS, Oliveira MC, Santos TO, Rufino LRA, Oliveira NMS (2021) Incidence of Shiga toxin-producing *Escherichia coli* in diarrheic calves and its susceptibility profile to antimicrobials and *Eugenia uniflora* L. Can J Vet Res 85(1):18–26

Caballero-Prado CJ, Merino-Mascorro JA, Heredia N, Davila-Avina J, Garcia S (2021) Eugenol, citral, and hexanal, alone or in combination with heat, affect viability, biofilm formation, and swarming on Shiga-toxin-producing *Escherichia coli*. Food Sci Biotechnol 30(4):599–607. https://doi.org/10.1007/s10068-021-00887-y

Cada DJ, Baker DE (2014) Oritavancin diphosphate. Hosp Pharm 49(11):1049–1060. https://doi.org/10.1310/hpj4911-1049

Carter MQ, Quinones B, Laniohan N et al (2023) Pathogenicity assessment of Shiga toxin-producing *Escherichia coli* strains isolated from wild birds

in a major agricultural region in California. Front Microbiol 14:1214081. https://doi.org/10.3389/fmicb.2023.1214081

Chase-Topping M, Dallman TJ, Allison L et al (2023) Analysis of *Escherichia coli* O157 strains in cattle and humans between Scotland and England & Wales: implications for human health. Microb Genom. https://doi.org/10.1099/mgen.0.001090

Chen CH, Lu TK (2020) Development and challenges of antimicrobial peptides for therapeutic applications. Antibiotics (basel). https://doi.org/10.3390/antibiotics9010024

Colovos C, Yeates TO (1993) Verification of protein structures: patterns of nonbonded atomic interactions. Protein Sci 2(9):1511–1519. https://doi.org/10.1002/pro.5560020916

Comeau SR, Gatchell DW, Vajda S, Camacho CJ (2004) ClusPro: a fully automated algorithm for protein-protein docking. Nucleic Acids Res 32(Web Server issue):W96–W99. https://doi.org/10.1093/nar/gkh354

Crane JK, Salehi M, Alvarado CL (2021) Psychoactive drugs induce the SOS response and Shiga toxin production in *Escherichia coli*. Toxins (basel). https://doi.org/10.3390/toxins13070437

Dallakyan S, Olson AJ (2015) Small-molecule library screening by docking with PyRx. Methods Mol Biol 1263:243–250. https://doi.org/10.1007/978-1-4939-2269-7_19

de Virgilio M, Lombardi A, Caliandro R, Fabbrini MS (2010) Ribosome-inactivating proteins: from plant defense to tumor attack. Toxins (basel) 2(11):2699–2737. https://doi.org/10.3390/toxins2112699

Deep A, Grakh K et al (2023) Molecular epidemiology, antibiogram profile and risk factor analysis of pathogenic *Escherichia coli* associated with pre-weaning diarrhoea in piglets from Haryana, India. J Infect Public Health 16(11):1793–1801. https://doi.org/10.1016/j.jiph.2023.08.019

Di R, Kyu E, Shete V, Saidasan H, Kahn PC, Tumer NE (2011) Identification of amino acids critical for the cytotoxicity of Shiga toxin 1 and 2 in *Saccharomyces cerevisiae*. Toxicon 57(4):525–539. https://doi.org/10.1016/j.toxicon.2010.12.006

Doytchinova IA, Flower DR (2007) VaxiJen: a server for prediction of protective antigens, tumour antigens and subunit vaccines. BMC Bioinform 8:4. https://doi.org/10.1186/1471-2105-8-4

El-Bastawisy HS, El-Sayyad GS, Abu Safe FA (2023) Detection of hemolytic Shiga toxin-producing *Escherichia coli* in fresh vegetables and efficiency of phytogenically synthesized silver nanoparticles by *Syzygium aromaticum* extract and gamma radiation against isolated pathogens. BMC Microbiol 23(1):262. https://doi.org/10.1186/s12866-023-02994-8

Fernandez M, Casaux ML, Fraga M et al (2023) Shiga toxin-producing *Escherichia coli* (STEC) associated with calf mortality in Uruguay. Microorganisms. https://doi.org/10.3390/microorganisms11071704

Fitzgerald SF, Mitchell MC, Holmes A et al (2023) Prevalence of Shiga toxin-producing *Escherichia coli* O157 in wild Scottish deer with high human pathogenic potential. Animals (basel). https://doi.org/10.3390/ani13172795

Freedman SB, van de Kar N, Tarr PI (2023) Shiga toxin-producing *Escherichia coli* and the hemolytic-uremic syndrome. N Engl J Med 389(15):1402–1414. https://doi.org/10.1056/NEJMra2108739

Gallo RL, Nizet V (2003) Endogenous production of antimicrobial peptides in innate immunity and human disease. Curr Allergy Asthma Rep 3(5):402–409. https://doi.org/10.1007/s11882-003-0074-x

Gasteiger E, Gattiker A, Hoogland C, Ivanyi I, Appel RD, Bairoch A (2003) ExPASy: the proteomics server for in-depth protein knowledge and analysis. Nucleic Acids Res 31(13):3784–3788. https://doi.org/10.1093/nar/gkg563

Geourjon C, Deleage G (1995) SOPMA: significant improvements in protein secondary structure prediction by consensus prediction from multiple alignments. Comput Appl Biosci 11(6):681–684. https://doi.org/10.1093/bioinformatics/11.6.681

Goodman RE, Ebisawa M, Ferreira F et al (2016) AllergenOnline: a peer-reviewed, curated allergen database to assess novel food proteins for potential cross-reactivity. Mol Nutr Food Res 60(5):1183–1198. https://doi.org/10.1002/mnfr.201500769

Gupta S, Kapoor P, Chaudhary K et al (2013) In silico approach for predicting toxicity of peptides and proteins. PLoS ONE 8(9):e73957. https://doi.org/10.1371/journal.pone.0073957

Henrique IM, Sacerdoti F, Ferreira RL et al (2022) Therapeutic antibodies against Shiga toxins: trends and perspectives. Front Cell Infect Microbiol 12:825856. https://doi.org/10.3389/fcimb.2022.825856

Heydari FE, Bonyadian M, Moshtaghi H, Sami M (2020) Prevalence and antibiotic resistance profile of Shiga toxin-producing *Escherichia coli* isolated from diarrheal samples. Iran J Microbiol 12(4):289–295. https://doi.org/10.18502/ijm.v12i4.3931

Hwang SB, Chelliah R, Kang JE et al (2021) Role of recent therapeutic applications and the infection strategies of Shiga toxin-producing *Escherichia coli*. Front Cell Infect Microbiol 11:614963. https://doi.org/10.3389/fcimb.2021.614963

Jones G, Mariani-Kurkdjian P, Cointe A et al (2023) Sporadic Shiga toxin-producing *Escherichia coli*-associated pediatric hemolytic uremic syndrome, France, 2012–2021. Emerg Infect Dis 29(10):2054–2064. https://doi.org/10.3201/eid2910.230382

Kakoullis L, Papachristodoulou E, Chra P, Panos G (2019) Shiga toxin-induced haemolytic uraemic syndrome and the role of antibiotics: a global overview. J Infect 79(2):75–94. https://doi.org/10.1016/j.jinf.2019.05.018

Ko J, Park H, Heo L, Seok C (2012) GalaxyWEB server for protein structure prediction and refinement. Nucleic Acids Res 40(Web Server issue):W294–W297. https://doi.org/10.1093/nar/gks493

Kumar GD, Oguadinma IC, Mishra A, Suh JH, Singh M (2023) Influence of antibiotic-resistance and exudate on peroxyacetic acid tolerance in O157 and non-O157 Shiga toxin producing *E. coli*. Int J Food Microbiol 391–393:110144. https://doi.org/10.1016/j.ijfoodmicro.2023.110144

Laskowski RA, Rullmannn JA, MacArthur MW, Kaptein R, Thornton JM (1996) AQUA and PROCHECK-NMR: programs for checking the quality of protein structures solved by NMR. J Biomol NMR 8(4):477–486. https://doi.org/10.1007/BF00228148

Lee KS, Park JY, Jeong YJ, Lee MS (2023) The fatal role of enterohaemorrhagic *Escherichia coli* Shiga toxin-associated extracellular vesicles in host cells. J Microbiol 61(8):715–727. https://doi.org/10.1007/s12275-023-00066-0

Li XP, Tumer NE (2017) Differences in ribosome binding and sarcin/ricin loop depurination by Shiga and ricin holotoxins. Toxins (basel). https://doi.org/10.3390/toxins9040133

Li T, Tu W, Liu Y et al (2016) A potential therapeutic peptide-based neutralizer that potently inhibits Shiga toxin 2 in vitro and in vivo. Sci Rep 6:21837. https://doi.org/10.1038/srep21837

Lino M, Kus JV, Tran SL et al (2011) A novel antimicrobial peptide significantly enhances acid-induced killing of Shiga toxin-producing *Escherichia coli* O157 and non-O157 serotypes. Microbiology (reading) 157(Pt 6):1768–1775. https://doi.org/10.1099/mic.0.047365-0

Liu G, Li C, Liao S, Guo A, Wu B, Chen H (2023) C500 variants conveying complete mucosal immunity against fatal infections of pigs with *Salmonella enterica* serovar Choleraesuis C78–1 or F18+ Shiga toxin-producing *Escherichia coli*. Front Microbiol 14:1210358. https://doi.org/10.3389/fmicb.2023.1210358

Liu Y, Thaker H, Wang C, Xu Z, Dong M (2022) Diagnosis and treatment for Shiga toxin-producing escherichia coli associated hemolytic uremic syndrome. Toxins (basel). https://doi.org/10.3390/toxins15010010

Lopez-Blanco JR, Aliaga JI, Quintana-Orti ES, Chacon P (2014) iMODS: internal coordinates normal mode analysis server. Nucleic Acids Res 42(Web Server issue):W271–W327. https://doi.org/10.1093/nar/gku339

Massari ME, Murre C (2000) Helix-loop-helix proteins: regulators of transcription in eucaryotic organisms. Mol Cell Biol 20(2):429–440. https://doi.org/10.1128/MCB.20.2.429-440.2000

Melo F, Devos D, Depiereux E, Feytmans E (1997) ANOLEA: a www server to assess protein structures. Proc Int Conf Intell Syst Mol Biol 5:187–190

Milton AAP, Srinivas K, Lyngdoh V et al (2023) Biofilm-forming antimicrobial-resistant pathogenic *Escherichia coli*: a one health challenge in Northeast India. Heliyon 9(9):e20059. https://doi.org/10.1016/j.heliyon.2023.e20059

Mir RA, Kudva IT (2019) Antibiotic-resistant Shiga toxin-producing *Escherichia coli*: an overview of prevalence and intervention strategies. Zoonoses Public Health 66(1):1–13. https://doi.org/10.1111/zph.12533

Muhlen S, Dersch P (2020) Treatment strategies for infections with Shiga toxin-producing *Escherichia coli*. Front Cell Infect Microbiol 10:169. https://doi.org/10.3389/fcimb.2020.00169

Necel A, Bloch S, Topka-Bielecka G et al (2022) Synergistic effects of bacteriophage vB_Eco4-M7 and selected antibiotics on the biofilm formed by shiga toxin-producing *Escherichia coli*. Antibiotics (basel). https://doi.org/10.3390/antibiotics11060712

Neu C, Wissuwa B, Thiemermann C, Coldewey SM (2023) Cardiovascular impairment in Shiga-toxin-2-induced experimental hemolytic-uremic

syndrome: a pilot study. Front Immunol 14:1252818. https://doi.org/10.3389/fimmu.2023.1252818

Nishikawa K, Watanabe M, Kita E et al (2006) A multivalent peptide library approach identifies a novel Shiga toxin inhibitor that induces aberrant cellular transport of the toxin. FASEB J 20(14):2597–2599. https://doi.org/10.1096/fj.06-6572fje

Obata F, Ozuru R, Tsuji T, Matsuba T, Fujii J (2022) Stx2 induces differential gene expression and disturbs circadian rhythm genes in the proximal tubule. Toxins (basel). https://doi.org/10.3390/toxins14020069

Oguadinma I, Mishra A, Dev Kumar G (2023) Antibiotic resistance associated lactic acid cross tolerance in Shiga-toxin producing *E. coli*. Front Microbiol 14:1059144. https://doi.org/10.3389/fmicb.2023.1059144

Pettersen EF, Goddard TD, Huang CC et al (2004) UCSF Chimera—a visualization system for exploratory research and analysis. J Comput Chem 25(13):1605–1612. https://doi.org/10.1002/jcc.20084

Prada-Prada S, Florez-Castillo J, Farfan-Garcia A, Guzman F, Hernandez-Penaranda I (2020) Antimicrobial activity of Ib-M peptides against *Escherichia coli* O157: H7. PLoS ONE 15(2):e0229019. https://doi.org/10.1371/journal.pone.0229019

Puno-Sarmiento J, Anderson EM, Park AJ, Khursigara CM, Barnett Foster DE (2020) Potentiation of antibiotics by a novel antimicrobial peptide against Shiga toxin producing *E. coli* O157:H7. Sci Rep 10(1):10029. https://doi.org/10.1038/s41598-020-66571-z

Rahal EA, Fadlallah SM, Nassar FJ, Kazzi N, Matar GM (2015) Approaches to treatment of emerging Shiga toxin-producing *Escherichia coli* infections highlighting the O104:H4 serotype. Front Cell Infect Microbiol 5:24. https://doi.org/10.3389/fcimb.2015.00024

Ramstad SN, Taxt AM, Naseer U, Wasteson Y, Bjornholt JV, Brandal LT (2021) Effects of antimicrobials on Shiga toxin production in high-virulent Shiga toxin-producing *Escherichia coli*. Microb Pathog 152:104636. https://doi.org/10.1016/j.micpath.2020.104636

Rubab M, Oh DH (2021) Molecular detection of antibiotic resistance genes in Shiga toxin-producing *E. coli* Isolated from different sources. Antibiotics (basel). https://doi.org/10.3390/antibiotics10040344

Rudolph MJ, Davis SA, Tumer NE, Li XP (2020) Structural basis for the interaction of Shiga toxin 2a with a C-terminal peptide of ribosomal P stalk proteins. J Biol Chem 295(46):15588–15596. https://doi.org/10.1074/jbc.AC120.015070

Sameer CA, Shah M, Nandy D, Gupta R (2023) Genomic index of sensitivity to chemotherapy for triple negative breast cancer. Asian Pac J Cancer Prev 24(6):2043–2053. https://doi.org/10.31557/APJCP.2023.24.6.2043

Spitznagel JK (1997) Origins and development of peptide antibiotic research. From extracts to abstracts to contracts. Methods Mol Biol 78:1–14. https://doi.org/10.1385/0-89603-408-9:1

Stearns-Kurosawa DJ, Collins V, Freeman S et al (2011) Rescue from lethal Shiga toxin 2-induced renal failure with a cell-permeable peptide. Pediatr Nephrol 26(11):2031–2039. https://doi.org/10.1007/s00467-011-1913-y

Suh JK, Hovde CJ, Robertus JD (1998) Shiga toxin attacks bacterial ribosomes as effectively as eucaryotic ribosomes. Biochemistry 37(26):9394–9398. https://doi.org/10.1021/bi980424u

Tang J, Lu X, Zhang T et al (2023) Shiga toxin 2 A-subunit induces mitochondrial damage, mitophagy and apoptosis via the interaction of Tom20 in Caco-2 cells. Heliyon 9(9):e20012. https://doi.org/10.1016/j.heliyon.2023.e20012

Tarr PI, Freedman SB (2022) Why antibiotics should not be used to treat Shiga toxin-producing *Escherichia coli* infections. Curr Opin Gastroenterol 38(1):30–38. https://doi.org/10.1097/MOG.0000000000000798

Thevenet P, Shen Y, Maupetit J, Guyon F, Derreumaux P, Tuffery P (2012) PEP-FOLD: an updated de novo structure prediction server for both linear and disulfide bonded cyclic peptides. Nucleic Acids Res 40(Web Server issue):W288–W293. https://doi.org/10.1093/nar/gks419

Tian W, Chen C, Lei X, Zhao J, Liang J (2018) CASTp 3.0: computed atlas of surface topography of proteins. Nucleic Acids Res 46(W1):W363–W367. https://doi.org/10.1093/nar/gky473

Watanabe-Takahashi M, Tamada M, Senda M et al (2021) Identification of a peptide motif that potently inhibits two functionally distinct subunits of Shiga toxin. Commun Biol 4(1):538. https://doi.org/10.1038/s42003-021-02068-3

Wilkins MR, Gasteiger E, Bairoch A et al (1999) Protein identification and analysis tools in the ExPASy server. Methods Mol Biol 112:531–552. https://doi.org/10.1385/1-59259-584-7:531

## Publisher's Note